

# Folding transitions in three–dimensional space with defects

Emilio N.M. Cirillo,<sup>1,\*</sup> Giuseppe Gonnella,<sup>2,†</sup> and Alessandro Pelizzola<sup>3,4,5,‡</sup>

<sup>1</sup>*Dipartimento di Scienze di Base e Applicate per l'Ingegneria,  
Sapienza Università di Roma, via A. Scarpa 16, I-00161, Roma, Italy.*

<sup>2</sup>*Dipartimento di Fisica dell'Università degli Studi di Bari,  
and INFN, Sezione di Bari, via Amendola 173, 70126 Bari, Italy.*

<sup>3</sup>*Dipartimento di Scienza Applicata e Tecnologia,  
CNISM and Center for Computational Studies, Politecnico di Torino,  
Corso Duca degli Abruzzi 24, I-10129 Torino, Italy*

<sup>4</sup>*INFN, Sezione di Torino, via Pietro Giuria 1, I-10125 Torino, Italy*

<sup>5</sup>*Human Genetics Foundation, HuGeF, Via Nizza 52, I-10126 Torino, Italy*

A model describing the three–dimensional folding of the triangular lattice on the face–centered cubic lattice is generalized allowing the presence of defects, which are related to cuts in the two–dimensional network. The model can be expressed in terms of Ising–like variables with nearest–neighbor and plaquette interactions in the hexagonal lattice; its phase diagram is determined by means of the Cluster Variation Method. The results found by varying the curvature and defect energy show that the introduction of defects turns the first–order crumpling transitions of the model without defects into continuous transitions. New phases also appear by decreasing the energy cost of defects and the behavior of their densities has been analyzed.

PACS numbers: 05.50.+q (Ising problems); 64.60.-i (General studies of phase transitions); 82.65.Dp (Thermodynamics of surfaces and interfaces)

Keywords: polymerized membranes, folding, defects, cluster variation method

## I. INTRODUCTION

The behavior of fluctuating membranes and surfaces is relevant for many physical and biological systems, from gauge theories and strings to vesicles and cellular membranes; see Refs. [1, 2] for reviews. A class is given by polymerized or crystalline membranes [3–5] consisting of two–dimensional networks of molecules with fixed connectivity. Examples are the spectrin network in red–blood cells [6] or the graphene [7]. Theoretical arguments suggest the relevance of curvature energy terms for the macroscopic behavior of fluctuating surfaces [1]. For polymerized membranes, at variance with fluid membranes [8], a flat phase with long–range order in the orientation of the normals to the surface is expected to be stable at high bending rigidity [9].

The prediction of a crumpling transition for *phantom* polymerized membranes (where self–avoidance is not taken into account) is confirmed on the basis of various analytical results [10–13] and numerical simulations [3, 14, 15] on continuous models. The character

of the transition is controversial. Among the most recent results, the simulations of Refs. [16] suggest a first–order behavior while the non–perturbative renormalization group calculations of [17] predict for a phantom membrane embedded in the three–dimensional space a continuous transition.

A different approach has been to study discrete models for polymerized membranes whose nodes are constrained to occupy positions corresponding to the sites of a given lattice. Solutions of discrete models, as in other domains of statistical physics, can represent a reference for the behavior of fluctuating membranes of a given class. It is well–known that Ising–like models [18, 19] naturally admit an interpretation in terms of a surface gas with a variable number of components. More difficult is the problem of representing a single membrane in terms of discrete variables. In Ref. [20] Bowick and co–workers have been able to model the folding of a triangular network in the face–centered cubic (fcc) lattice in terms of local discrete variables, subject to local constraints. Since the distance between the nodes of the network is fixed, in this model one can consider as frozen the “phonon” degrees of freedom of the membrane while only the bending modes are taken into account [21]. A simpler version of the folding problem of [20] has been studied in [22–25]

\* emilio.cirillo@uniroma1.it; corresponding author.

† Giuseppe.Gonnella@ba.infn.it

‡ alessandro.pelizzola@polito.it

corresponding to the case of a two-dimensional embedding space. Here the normals to the triangles of the network can point only “up” or “down” in some direction. A similar model concerning the folding properties of a square lattice along the main axis and the diagonals has been studied in [26, 27]. Finally, the three-dimensional folding problems of the triangular lattice with quenched random bending rigidity and spontaneous curvature have been also respectively studied in [28] and [29].

The phase diagram of the model of [20] has been first studied in [30] and [31] by the cluster variation method (CVM) [32]. A sequence of transitions from the flat to the piled-up phase through the partially folded octahedral and tetrahedral phases was found by varying the bending rigidity from  $\infty$  to  $-\infty$ . The density-matrix renormalization group (DMRG) calculations of [33, 34] have confirmed the occurrence of these transitions. Both CVM and DMRG have predicted first-order flat-octahedral and octahedral-tetrahedral transitions while the character of the third transition is controversial. CVM suggested a continuous tetrahedral piled-up phase transition at variance with the weak first-order behavior predicted by DMRG.

In order to further analyze the character of the crumpling transitions of the triangular network in the fcc lattice, a modified folding rule allowing defects in the network has been introduced in [35]. Transfer-matrix calculations of [35] confirmed the order of the transitions given by DMRG.

In the present work we observe that the model of folding with defects is interesting by itself. Relaxing the local constraints on the Ising variables in the model of Ref. [20] corresponds to accepting folding configurations with bending and/or meeting points in the folding lines, which can be obtained by allowing cuts between adjacent triangles. Therefore the model with progressively relaxed constraints can describe polymerized membranes with an increasing number of defects in the connectivity rules. Here we will introduce such a model and study its equilibrium properties by means of the CVM.

The paper is organized as follows. In the next section we will introduce the model and describe the CVM approximation scheme used for studying it. Our results for the phase diagram and the equilibrium behavior of the most important quantities are reported in Sect. III. Conclusions will complete the paper.

## II. THE MODEL AND THE METHOD

The model for the folding of the triangular lattice in the three-dimensional fcc lattice has been introduced in [20, 30, 31].

In this model, sites of the triangular lattice are mapped onto sites of the fcc lattice, with the condition that two sites that are nearest-neighbors (NNs) in the triangular lattice must remain NNs in the fcc lattice. Let us consider two adjacent plaquettes of the triangular lattice, and call  $\theta$  the angle formed by their normal vectors (defined in such a way that  $\theta$  always vanishes in the planar configuration). It is easy to see that upon mapping onto the fcc lattice, the two plaquettes will be in one of four relative orientations, namely: (i) no fold, with  $\theta = 0, \cos \theta = 1$ ; (ii) octahedral fold, with  $\cos \theta = 1/3$  (the two plaquettes belong to the same octahedron in the fcc lattice); (iii) tetrahedral fold, with  $\cos \theta = -1/3$  (they belong to the same tetrahedron in the fcc lattice); (iv) complete fold, with  $\cos \theta = -1$  (they are on top of each other). A fold between two adjacent plaquettes has an energy cost, due to curvature, given by  $-K \cos \theta$ .

The model allows various representations [20], a particularly convenient one for our purposes being defined in terms of 2 sets of Ising variables. These variables are usually denoted by  $\sigma_i$  and  $z_i$ , the pair  $(\sigma_i, z_i)$  being associated to a plaquette of the triangular lattice or, equivalently, to a site  $i$  of the dual hexagonal lattice  $\Lambda$ . Sites of  $\Lambda$  correspond to plaquette centers in the triangular lattice, while edges of  $\Lambda$  are perpendicular to the edges of the triangular lattice. In terms of these Ising variables, the fold between two adjacent plaquettes 1 and 2 (corresponding to two NN sites in  $\Lambda$ ) is specified by the values  $\sigma_1 \sigma_2$  and  $z_1 z_2$  according to Tab. I, and the angle  $\theta$  is given by

$$\cos \theta = \sigma_1 \sigma_2 \frac{1 + 2z_1 z_2}{3}. \quad (2.1)$$

In the language of magnetism, we can say that different folds correspond to different types of domain walls for our Ising variables.

However, not all configurations of our Ising variables are allowed. It has been shown in [20] that the variables  $z_i$  and  $\sigma_i$  have to satisfy two constraints, or folding rules, in order to describe a proper folding configuration over the fcc lattice. Given an hexagon  $e$  in the set  $E$  of all the elementary plaquettes in  $\Lambda$ , let  $1, \dots, 6$  be its six sites ordered counterclockwise,  $\sigma_e = \{\sigma_i, i = 1, \dots, 6\}$  and

| Type of fold  | $\cos \theta$ | $\sigma_1 \sigma_2$ | $z_1 z_2$ |
|---------------|---------------|---------------------|-----------|
| no fold       | +1            | +1                  | +1        |
| octahedral    | +1/3          | -1                  | -1        |
| tetrahedral   | -1/3          | +1                  | -1        |
| complete fold | -1            | -1                  | +1        |

TABLE I. Type of folds and their representation in terms of Ising variables.

$z_e = \{z_i, i = 1, \dots, 6\}$ . Set

$$L(\sigma_e) = \sum_{i=1}^6 \sigma_i \quad (2.2)$$

and

$$M_c(\sigma_e, z_e) = \sum_{i=1}^6 \frac{1 - z_i z_{i+1}}{2} \Delta_{i,c}(\sigma_e) \quad (2.3)$$

where  $z_7 = z_1$  and

$$\Delta_{i,c}(\sigma_e) = \begin{cases} 1 & \text{if } \sum_{j=1}^i \sigma_j = c \pmod{3} \\ 0 & \text{otherwise} \end{cases} \quad (2.4)$$

with  $i = 1, \dots, 6$  and  $c = 1, 2$ . The folding rules then read

$$L(\sigma_e) = 0 \pmod{3} \quad (2.5)$$

$$M_c(\sigma_e, z_e) = 0 \pmod{2}, \quad c = 1, 2, 3. \quad (2.6)$$

Notice that  $M_1(\sigma_e, z_e) + M_2(\sigma_e, z_e) + M_3(\sigma_e, z_e)$  is an even number, and therefore the number of violated constraints in 2.6 can be only 0 or 2: as a consequence, it is sufficient to impose only 2 of the 3 conditions in 2.6.

We now introduce defects in the configurations of the triangular lattice. A violation of the folding rules Eqs.(2.5), (2.6) at a hexagon represents a defect at that hexagon.

The folding rules Eqs.(2.5) and (2.6) ensure that after a complete turn around any set of six triangles with a common vertex the triangles occupy the same absolute position [20]. Clearly, defects alter the local connectivity of the original triangular lattice and can be associated to cuts in the lattice. More specifically, defects can be associated to certain kinds of bending and/or meeting points of the various domain walls for the  $(\sigma, z)$  variables, which are not allowed in the original folding model and therefore do not appear in the set of allowed vertices in Fig. 10 of [20].

In Fig. 1, for example, we have a hexagon configuration containing only a domain wall between  $(\sigma, z) = (+1, +1)$

and  $(-1, +1)$  (we call it a complete-fold domain wall), which shows a bend at the center of the hexagon. This corresponds to a violation of constraint (2.5) only, as one can easily check. This configuration cannot appear in a fold of the triangular lattice, unless one allows cuts. It is however immediately evident that, at least locally, there are three possible ways to cut the hexagon. One can select one of the three edges of triangle number 6, cut the remaining two edges, and then fold the triangle along the selected edge. If this were the only defect in the whole configuration, this argument would apply globally as well. Therefore, already on the basis of this example, it is clear that a unique reconstruction of the surface is not feasible in the presence of defects.

The analysis of a similar configuration with  $(\sigma_i, z_i) = (+1, +1), i = 1, \dots, 5$  and  $(\sigma_6, z_6) = (-1, -1)$ , representing the bending of an octahedral-fold domain wall shows that in this case both constraints (2.5) and (2.6) are violated. On the other hand, in the case of bending of a tetrahedral-fold domain wall between  $(\sigma, z) = (+1, +1)$  and  $(+1, -1)$ , only (2.6) would be violated. On the basis of the previous examples one might be tempted to consider a specific geometrical interpretation for the separate violation of each of the two folding rules. This other example, however, shows that this interpretation would be problematic. In Fig. 2, we see a configuration where an octahedral-fold domain wall meets (ending at the meeting point) another domain wall, which at the meeting point changes its character from tetrahedral to complete: in this case both constraints (2.5) and (2.6) are violated. If, however, the complete and octahedral domain walls are swapped, only (2.5) is violated. One can conclude from the above examples that the two folding rules can not be directly associated to definite classes of defects.

Due to the above observation, we do not find reasons to attribute different energy costs to different kinds of defects and will consider a model where all defects are weighted in the same way [36]. A single energy parameter  $\lambda$  will be coupled to the number of defects, that is the number of hexagons at which (one or more) constraints are violated. Taking also into account Eq. (2.1) for writing the curvature energy as in [30], we are led to consider

the Hamiltonian (energies are given in units of  $k_B T$ )

$$\begin{aligned}
H = & -\frac{K}{3} \sum_{\langle ij \rangle} \sigma_i \sigma_j (1 + 2z_i z_j) \\
& -\lambda \sum_{e \in E} \left[ \mathbb{I}_{\{L(\sigma_e)=0 \bmod 3\}} \right. \\
& \quad \left. \times \prod_{c=1}^3 \mathbb{I}_{\{M_c(\sigma_e, z_e)=0 \bmod 2\}} \right]
\end{aligned} \tag{2.7}$$

where  $\mathbb{I}_{\{\text{condition}\}}$  is equal to one if the condition is satisfied and to zero otherwise. Note that in the above formula the first sum is extended to the NN pairs and the second to the hexagons of the lattice. Moreover, the product over the three color indices in the last sum is redundant: according to our discussion of constraints (2.6), it is sufficient to impose only 2 of the 3 constraints.

Finally, we observe that it is not possible to express the energy cost of defects in terms of local weights for the length of the cuts needed to obtain a surface realization of a given  $(\sigma, z)$  configuration. This can be shown by the following example. Consider a set of 3 defects corresponding to  $60^\circ$  bends of complete-fold domain walls as those shown in Fig. 1. These defects can be used to construct configurations where a complete-fold domain wall can form equilateral triangles of any size,  $(\sigma, z) = (+1, +1)$  outside the triangle, and  $(\sigma, z) = (-1, +1)$  inside it. Hence, given the same set of 3 defects, one can construct configurations corresponding to cuts of any size.

As it was done for the two-dimensional model discussed in [24] and for the defect free three-dimensional case studied in [30], the phase diagram will be investigated by means of the hexagon approximation of the CVM. For the sake of self-containedness we briefly recall the main features of our approach.

We recall that  $E$  is the collection of hexagons on the lattice. We denote by  $M$  the collections of all the hexagons and all their sub-clusters (site subsets). To each cluster  $\alpha \in M$  a probability distribution  $\rho_\alpha(\sigma_\alpha, z_\alpha)$  is associated, where  $\sigma_\alpha = \{\sigma_i, i \in \alpha\}$  and  $z_\alpha = \{z_i, i \in \alpha\}$ . In this CVM approximation the free energy functional is given by

$$\begin{aligned}
F_M = & \sum_{\alpha \in M} \sum_{\sigma_\alpha, z_\alpha} H_\alpha(\sigma_\alpha, z_\alpha) \rho_\alpha(\sigma_\alpha, z_\alpha) \\
& + \sum_{\alpha \in M} a_\alpha \sum_{\sigma_\alpha, z_\alpha} \rho_\alpha(\sigma_\alpha, z_\alpha) \log \rho_\alpha(\sigma_\alpha, z_\alpha),
\end{aligned} \tag{2.8}$$

where the coefficients  $a_\alpha$  are such that for each  $\alpha \in M$

$$\sum_{\beta \in M: \beta \supseteq \alpha} a_\beta = 1 \tag{2.9}$$

and the Hamiltonian terms  $H_\alpha$  are defined as follows: for a cluster made of two neighboring sites  $\langle i, j \rangle$  we have

$$H_{\langle i, j \rangle} = -\frac{K}{3} \sigma_i \sigma_j (1 + 2z_i z_j),$$

for a cluster made of a hexagon  $e \in E$

$$H_e = -\lambda \mathbb{I}_{\{L(\sigma_e)=0 \bmod 3\}} \prod_{c=1}^2 \mathbb{I}_{\{M_c(\sigma_e, z_e)=0 \bmod 2\}}$$

and  $H_\alpha = 0$  otherwise. By using Eq. (2.9) it is not difficult to prove that the sole non-vanishing coefficients  $a_\alpha$  are those associated to hexagons, NN pairs, and single sites; coefficients associated to five-site, four-site, three-site, and not neighboring two-site clusters are all equal to zero. In particular we have that

$$a_e = 1, \quad a_{\langle i, j \rangle} = -1, \quad \text{and} \quad a_i = 1$$

for each hexagon  $e \in E$ , each nearest-neighbor pair  $\langle i, j \rangle$ , and each site  $i \in \Lambda$ .

We now exploit the translational invariance of the system, which implies that all the probability distributions associated to a particular sub-family of clusters in  $M$  are equal. Thus, we denote by  $\rho_6(\sigma_1, \dots, \sigma_6, z_1, \dots, z_6)$  the probability distribution associated to hexagons and by  $\rho_2(\sigma_1, \sigma_2, z_1, z_2)$  that associated to NN pairs. Site clusters form two sub-families: indeed, a hexagonal lattice is a bipartite lattice, made of two inter-penetrating (triangular) sub-lattices  $a$  and  $b$ , such that all the NNs of a site in  $a$  belong to  $b$  and vice-versa. Since we expect the symmetry between the two sub-lattices to be broken in some thermodynamic phases of the model, it is important to distinguish the site probability distributions corresponding to  $a$  and  $b$ . For the same reason, in the argument of  $\rho_2$ , the first and the third entries ( $\sigma_1$  and  $z_1$ ) refer to sub-lattice  $a$ , while the second and the fourth ones ( $\sigma_2$  and  $z_2$ ) refer to sub-lattice  $b$ , and they cannot be interchanged.

With the above definitions and notations, and observing that the number of hexagons and NN pairs in  $\Lambda$  are respectively  $N_6 = |\Lambda|/2$  and  $N_2 = 3|\Lambda|/2$ , from Eq. (2.8) we obtain the following expression for the CVM free energy density functional  $f = F_M/|\Lambda|$ :

$$f = -\frac{1}{2}K\text{Tr}_2[\sigma_1\sigma_2(1+2z_1z_2)\rho_2] - \frac{1}{2}\text{Tr}_6\left[\left(\lambda\mathbb{I}_{\{L(\sigma_e)=0 \bmod 3\}}\prod_{c=1}^2\mathbb{I}_{\{M_c(\sigma_e,z_e)=0 \bmod 2\}}\right)\rho_6\right] \quad (2.10)$$

$$+ \frac{1}{2}\text{Tr}_6[\rho_6 \ln \rho_6] - \frac{3}{2}\text{Tr}_2[\rho_2 \ln \rho_2] + \frac{1}{2}\text{Tr}_1[\rho_{1,a} \ln \rho_{1,a}] + \frac{1}{2}\text{Tr}_1[\rho_{1,b} \ln \rho_{1,b}] + \nu(\text{Tr}_6\rho_6 - 1),$$

where we have introduced the notation

$$\text{Tr}_6 = \sum_{\substack{\sigma_1, \dots, \sigma_6 \\ z_1, \dots, z_6}}, \quad \text{Tr}_2 = \sum_{\substack{\sigma_1, \sigma_2 \\ z_1, z_2}}, \quad \text{Tr}_1 = \sum_{\sigma_1, z_1},$$

and  $\nu$  is a Lagrange multiplier which ensures the normal-

ization of  $\rho_6$ . The other probability distributions do not need a normalization constraint since they can be written as partial traces of probability distributions of larger clusters. More precisely,

$$\rho_2(\sigma_1, \sigma_2, z_1, z_2) = \frac{1}{6} \sum_{\substack{\sigma_3, \dots, \sigma_6 \\ z_3, \dots, z_6}} [\rho_6(\sigma_1, \sigma_2, \sigma_3, \sigma_4, \sigma_5, \sigma_6, \dots) + \rho_6(\sigma_3, \sigma_2, \sigma_1, \sigma_4, \sigma_5, \sigma_6, \dots) + \rho_6(\sigma_3, \sigma_4, \sigma_1, \sigma_2, \sigma_5, \sigma_6, \dots) + \rho_6(\sigma_3, \sigma_4, \sigma_5, \sigma_2, \sigma_1, \sigma_6, \dots) + \rho_6(\sigma_3, \sigma_4, \sigma_5, \sigma_6, \sigma_1, \sigma_2, \dots) + \rho_6(\sigma_1, \sigma_4, \sigma_5, \sigma_6, \sigma_3, \sigma_2, \dots)] \quad (2.11)$$

where the  $z$  variables in the argument of  $\rho_6$  appear in the same order as  $\sigma$  variables, and

$$\rho_{1,a}(\sigma_1, z_1) = \sum_{\sigma_2, z_2} \rho_2(\sigma_1, \sigma_2, z_1, z_2), \quad (2.12)$$

$$\rho_{1,b}(\sigma_2, z_2) = \sum_{\sigma_1, z_1} \rho_2(\sigma_1, \sigma_2, z_1, z_2). \quad (2.13)$$

With the above definitions the CVM free energy density functional  $f$  can be regarded as a function of  $\rho_6$

only. The minimization must be performed numerically, and this can be easily done by standard iterative methods as in [24] (see [32] for a survey of such algorithms). The simplest possibility is to write stationarity equations by taking derivatives of  $f$  with respect to an element of  $\rho_6(\sigma_1, \dots, \sigma_6, z_1, \dots, z_6)$ , for some generic choice  $\sigma_1, \dots, \sigma_6, z_1, \dots, z_6 = \pm 1$  of the spin variables and letting  $\sigma_7 = \sigma_1$  and  $z_7 = z_1$ . After some algebra, we get

$$\rho_6(\sigma_1, \dots, \sigma_6, z_1, \dots, z_6) = \exp\left\{(K/6) \sum_{i=1}^6 \sigma_i \sigma_{i+1} (1 + 2z_i z_{i+1}) - 2\nu + \lambda \mathbb{I}_{\{L(\sigma_e)=0 \bmod 3\}} \prod_{c=1}^2 \mathbb{I}_{\{M_c(\sigma_e, z_e)=0 \bmod 2\}}\right\} \quad (2.14)$$

$$\times [\rho_2(\sigma_1, \sigma_2, z_1, z_2) \rho_2(\sigma_3, \sigma_2, z_3, z_2) \rho_2(\sigma_3, \sigma_4, z_3, z_4) \rho_2(\sigma_5, \sigma_4, z_5, z_4) \rho_2(\sigma_5, \sigma_6, z_5, z_6) \rho_2(\sigma_1, \sigma_6, z_1, z_6)]^{1/2}$$

$$\times [\rho_{1,a}(\sigma_1, z_1) \rho_{1,b}(\sigma_2, z_2) \rho_{1,a}(\sigma_3, z_3) \rho_{1,b}(\sigma_4, z_4) \rho_{1,a}(\sigma_5, z_5) \rho_{1,b}(\sigma_6, z_6)]^{-1/3}$$

that can be solved numerically with an iterative approach.

### III. RESULTS

We now present our results for the phase diagram of

the folding model Eq. (2.7), obtained by finding the stable (lowest free energy) solutions of Eq. (2.14) at varying curvature energy and defect cost. Following [31] we introduce the order parameters  $\mathbf{O} \equiv \langle \sigma_i^{\text{st}} \rangle$ ,  $\mathbf{T} \equiv \langle z_i \sigma_i^{\text{st}} \rangle$  and  $\mathbf{P} \equiv \langle \sigma_i^{\text{st}} \rangle$ .  $\mathbf{O}$  and  $\mathbf{T}$  were named octahedral and tetrahedral order parameters, respectively, and indeed they are the only order parameters which become non-zero in the

| Phase        | <b>M</b> | <b>P</b> | <b>N</b> | <b>O</b> | <b>T</b> |
|--------------|----------|----------|----------|----------|----------|
| flat         | $\neq 0$ | $\neq 0$ | $\neq 0$ | 0        | 0        |
| p-octahedral | 0        | 0        | 0        | $\neq 0$ | 0        |
| tetrahedral  | 0        | 0        | 0        | 0        | $\neq 0$ |
| piled-up     | 0        | $\neq 0$ | 0        | $\neq 0$ | $\neq 0$ |
| f-octahedral | 0        | 0        | $\neq 0$ | 0        | 0        |
| disordered   | 0        | 0        | 0        | 0        | 0        |

TABLE II. Phases. In the first column the name of the phase is reported. In the columns from the second to the sixth it is indicated which, among the order parameters  $\mathbf{M} = \langle \sigma_i \rangle$ ,  $\mathbf{P} = \langle z_i \rangle$ ,  $\mathbf{O} = \langle \sigma_i^{\text{st}} \rangle$ ,  $\mathbf{N} = \langle \sigma_i z_i \rangle$ , and  $\mathbf{T} = \langle \sigma_i^{\text{st}} z_i \rangle$ , differ from zero.

corresponding phases (observe, as explained later, that the octahedral phase of the model without defects will be called in this paper p-octahedral).  $\mathbf{P}$  was named planar order parameter, since it becomes non-zero in the planar (here called flat) phase. In order to characterize and distinguish all the phases we obtain here, it is convenient to define two additional order parameters,  $\mathbf{M} \equiv \langle \sigma_i \rangle$  and  $\mathbf{N} \equiv \langle z_i \sigma_i \rangle$ .  $\mathbf{M} = 1$  corresponds to configurations with tetrahedral folds or no folds only, while  $\mathbf{N} = 1$  corresponds to configurations with octahedral folds or no folds only.  $\mathbf{M}$  is non-zero only in the flat phase, while  $\mathbf{N}$  is non-zero in the flat and in the f-octahedral phase, as described later. The identification of the various phases of the model in terms of the above order parameters is summarized in Tab. II.

Fig. 3 summarizes our results for the phase diagram in the plane  $K$ - $\lambda$ . We shall describe it by first considering the large  $\lambda$  limit, where defects are absent and one recovers previous results [30, 31]. We shall then consider smaller values of  $\lambda$  in order to see how the various phases and phase transitions are modified by the introduction of defects.

At large enough  $\lambda$ , folding rules are practically never violated and the equilibrium thermodynamics of the model becomes independent of  $\lambda$ . Indeed, in the upper portion of the phase diagram Fig. 3, the phase transition lines are practically vertical and do not change their nature anymore. We can easily check that the results of the defect-free case [30, 31] are recovered in this limit. For instance, at  $\lambda = 20$  and vanishing  $K$  we obtain the entropy (per site)  $S = \ln q$ , where  $q = 1.42805$ , equal to the value obtained by the constrained CVM approach of [30] and in very good agreement with the transfer matrix estimate  $q = 1.43(1)$  of [20]. Furthermore we obtain

$\mathbf{O} = 0.87456$ ,  $\mathbf{M} = \mathbf{P} = \mathbf{N} = \mathbf{T} = 0$ , indicating a marked preference of the triangular lattice for wrapping on an octahedron at zero curvature cost. As already noticed in [31], here most folds between adjacent plaquettes are octahedral or complete. The sequence of folding transitions observed in the defect-free limit [30, 31] is reproduced here already at  $\lambda \gtrsim 4.91$ . Choosing  $\lambda = 10$  as an example, we find a flat phase at large  $K$  (in the limit  $\lambda \rightarrow \infty$  this phase is perfectly flat in this approximation), then at  $K = 0.1856$  a first-order transition occurs between the flat and the octahedral phases, characterized by  $\mathbf{M} = 0$ ,  $\mathbf{P} = 0$ ,  $\mathbf{N} = 0$ ,  $\mathbf{O} = 0.8247$ , and  $\mathbf{T} = 0$ . This phase, as shown in [31], is also characterized by a relative abundance of complete folds with respect to other folds. In order to make a difference with another phase appearing in the phase diagram (see the following) that is characterized by a relevant presence of octahedral folds, it will be called p(iled-up)-octahedral phase. Upon further decreasing  $K$  we find another first-order transition at  $K = -0.2940$  between the p-octahedral phase with  $\mathbf{M} = 0$ ,  $\mathbf{P} = 0$ ,  $\mathbf{N} = 0$ ,  $\mathbf{O} = 0.5816$ , and  $\mathbf{T} = 0$  and the tetrahedral one with  $\mathbf{M} = 0$ ,  $\mathbf{P} = 0$ ,  $\mathbf{N} = 0$ ,  $\mathbf{O} = 0$ , and  $\mathbf{T} = 0.7466$ . Finally, at  $K = -0.8395$  there is a continuous transition from the tetrahedral phase to the piled-up phase with the order parameters characterized by the continuous vanishing of  $\mathbf{P}$  and  $\mathbf{O}$ , while  $\mathbf{T} = 0.9993$ . This sequence of phases and phase transitions agrees in nature with that found in the defect-free limit [30, 31], providing a confirmation of the validity of the present approach.

Moving to lower values of  $\lambda$ , for  $\lambda \gtrsim 4.91$  the behavior described above remains qualitatively the same as in the case without defects, as it can be seen in Fig. 3. An illustration, for  $\lambda = 6$ , in terms of the order parameters as functions of  $K$ , is reported in the right column of Fig. 4.

By further decreasing the value of  $\lambda$  a new phase, characterized by the vanishing of all the order parameters, appears in the phase diagram. This phase, which we shall call disordered, is bounded by the tetrahedral and the p-octahedral phases at negative  $K$  and by the p-octahedral, the flat and the f-octahedral (see below) phases at positive  $K$ . The p-octahedral-disordered and tetrahedral-disordered phase transitions are continuous and the corresponding critical lines meet the p-octahedral-tetrahedral first-order transition line at a bicritical point at  $K = -0.298$ ,  $\lambda = 4.90$  (see Fig. 3). At positive  $K$ , the flat-disordered transition is first-order, like the flat-p-octahedral one, and the p-octahedral-

disordered critical line meets them at a critical end–point at  $K = 0.208$  and  $\lambda = 3.84$ . At zero curvature, the p–octahedral–disordered transition occurs at  $\lambda = 3.478$ . The behavior of the order parameters as a function of  $K$  at  $\lambda = 3.6$  is reported in the central column of Fig. 4.

Let us now proceed by describing our phase diagram at positive  $K$  and small  $\lambda$ . In this region another new phase, to be denoted by f(lat)–octahedral, is found between the disordered and the flat phase. The f–octahedral phase is characterized by  $\mathbf{N}$  being the only non–vanishing order parameter, while in terms of folds between adjacent plaquettes it exhibits a mixture of no–folds and octahedral folds. This can be seen in Fig. 5 where the average proportions of the four types of folds is shown as a function of  $K$ , for three values of  $\lambda$ ,  $\lambda = 0, 3.6$  and 6.

The appearance of the f–octahedral phase can be better understood by discussing the behavior of the model at  $\lambda = 0$ . As observed in [31], on this axis the model reduces to the Ashkin–Teller model [37], with parameters corresponding to the trivial case of two independent Ising models. Starting from low  $K$ , two continuous, symmetry breaking transitions are found. The first transition, separating the disordered phase from the f–octahedral phase, occurs at  $K = 3K_c/2$ , where  $K_c$  is the critical Ising coupling on the hexagonal lattice, as discussed in [31]. Here the order parameter  $\mathbf{N}$  becomes different from zero. The second transition, separating the f–octahedral phase from the flat phase, occurs at  $K = 3K_c$  [31]. Here the symmetries  $z \rightarrow -z$  and  $\sigma \rightarrow -\sigma$  are separately broken, and the order parameters  $\mathbf{M}$  and  $\mathbf{P}$  also become different from zero.

We find, in our approximation, that the two transitions occur at  $K_{c1} = 0.9321$  and at  $K_{c2} = 1.8642$ . These values correspond to the CVM estimate of the Ising critical point  $K_c = 0.6214$  on the hexagonal lattice (in the hexagonal plaquette approximation) [24]. At positive  $\lambda$  the transitions separating the f–octahedral and the disordered phases and the f–octahedral and the flat phases remain continuous. The corresponding lines meet at a bicritical point at  $K = 0.388$ ,  $\lambda = 2.39$  where the first–order disordered–flat transition appears.

At negative  $K$  the tetrahedral–piled–up phase transition remains continuous for all values of  $\lambda$ . The transition line intersects the horizontal axis at  $K = -K_{c2}$  where the symmetries  $z \rightarrow -z$  and  $\sigma_{st} \rightarrow -\sigma_{st}$  are separately broken. Moreover, at  $\lambda = 0$ , the disordered–tetrahedral continuous transition is found at  $K = -K_{c1}$ . These critical values correspond to the anti–ferromagnetic images of

the Ising transitions occurring in the equivalent Ashkin–Teller model at positive  $K$ . The behavior of the order parameters as a function of  $K$  at  $\lambda = 0$  is reported in the left column of Fig. 4.

The above results show that the introduction of defects turns first–order transition into continuous one, as in the planar folding case [24]. Here however the phase behavior is richer and we can observe an additional effect due to the presence of defects: the p–octahedral phase disappears, to be replaced by the disordered phase and the f–octahedral phase, which also exhibits a significant fraction of octahedral folds.

It is also worth taking a look at the number of defects appearing in our triangular lattice as a function of  $K$  and  $\lambda$ . To be more precise we define the fraction  $p_L$  of hexagons at which folding rule Eq. (2.5) is violated

$$p_L = \text{Tr}_6 \rho_6 \left( 1 - \mathbb{I}_{\{L(\sigma_e)=0 \bmod 3\}} \right), \quad (3.15)$$

the fractions  $p_{M_c}$  of hexagons at which folding rules Eq. (2.6) are violated

$$p_{M_c} = \text{Tr}_6 \rho_6 \left( 1 - \mathbb{I}_{\{M_c(\sigma_e, z_e)=0 \bmod 2\}} \right) \quad c = 1, 2 \quad (3.16)$$

and the fraction  $p$  of hexagons at which at least one folding rule is violated,

$$p = \text{Tr}_6 \rho_6 \left( 1 - \mathbb{I}_{\{M_c(\sigma_e, z_e)=0 \bmod 2\}} \times \prod_{c=1}^2 \mathbb{I}_{\{M_c(\sigma_e, z_e)=0 \bmod 2\}} \right). \quad (3.17)$$

These quantities are plotted as functions of  $K$  in Fig. 6 for  $\lambda = 6$  (that is, close to the defect–free limit), in Fig. 7 for  $\lambda = 3.6$ , and in Fig. 8 for  $\lambda = 0$ . We see that the fraction of defects has a maximum close to  $K = 0$  and decreases as  $|K|$  increases. Moreover, the fraction of defects is a decreasing function of  $\lambda$ . Considering the various phases we see that the phases exhibiting less fluctuations, namely the flat and piled–up phases, are almost defect–free, even at small  $\lambda$ , while the other phases are more prone to defects.

Notice also that  $p_{M_1}$  and  $p_{M_2}$  differ in the flat, p–octahedral and piled–up phases. This difference between  $p_{M_1}$  and  $p_{M_2}$  is a consequence of the breaking of the global inversion symmetry  $\sigma_i \rightarrow -\sigma_i, z_i \rightarrow -z_i, \forall i$ . This transformation maps configurations violating (2.6) for  $c = 1$  to configurations violating (2.6) for  $c = 2$ , and viceversa. The corresponding symmetry is preserved only in the disordered, f–octahedral and tetrahedral phases, where  $p_{M_1} = p_{M_2}$  as a consequence.

#### IV. CONCLUSIONS

We have generalized a model for the folding transitions of a triangular lattice in a three-dimensional space, discretized as a fcc lattice, by allowing defects corresponding to cuts in the triangular lattice, and weighing them by a suitable energy cost. We have studied the model in a six-point approximation of the CVM. In the limit of the energy cost of a defect going to  $+\infty$ , we recover previous results for the defect-free model [30, 31]. On the other hand, when this energy cost is sufficiently small, we find that first-order transitions are turned into continuous one, and that the octahedral phase found in the

defect-free limit, which was characterized by octahedral and complete folds between adjacent plaquettes, is replaced by a fully disordered phase and another phase characterized by octahedral folds and no-folds, which is related to the intermediate temperature phase of the Ashkin-Teller model. The model has a rich phase diagram with several multicritical points, namely, two bicritical points and a critical end-point. We have also shown that defects are more likely to occur in phases exhibiting larger fluctuations, while the flat and piled-up phases are almost defect free, and their concentration typically decreases as the absolute value of the curvature energy increases.

- 
- [1] *Statistical Mechanics of Membranes and Surfaces*, edited by D.R. Nelson, T. Piran, and S. Weinberg, (World Scientific, Singapore, 1989).
- [2] P. Ginsparg, F. David, and J. Zinn-Justin, *Fluctuating Geometries in Statistical Mechanics and Field Theories* (Elsevier Science, The Netherlands, 1996).
- [3] Y. Kantor, M. Kardar, and D.R. Nelson, Phys. Rev. Lett. **57**, 791 (1986); Phys. Rev. A **35**, 3056 (1987).
- [4] M.J. Bowick and A. Travesset, Phys. Rep. **344**, 255 (2001).
- [5] P. Di Francesco and E. Guitter, Phys. Rep. **415**, 1 (2005).
- [6] Y. Park et al., PNAS **107**, 1289 (2010).
- [7] A.H. Castro Neto, F. Guinea, N.M.R. Peres, K.S. Novoselov, and A.K. Geim, Rev. Mod. Phys. **81**, 109 (2009).
- [8] L. Peliti and S. Leibler, Phys. Rev. Lett. **54**, 1690 (1985).
- [9] D.R. Nelson and L. Peliti, J. Phys. (France) **48**, 1085 (1987).
- [10] F. David and E. Guitter, Europhys. Lett. **5**, 709 (1988).
- [11] M. Paczuski, M. Kardar, and D.R. Nelson, Phys. Rev. Lett. **60**, 2638 (1988); M. Paczuski and M. Kardar, Phys. Rev. A **39**, 6086 (1989).
- [12] J.A. Aronovitz and T.C. Lubensky, Phys. Rev. Lett. **60**, 2634 (1988).
- [13] P. Le Doussal and L. Radzihovsky, Phys. Rev. Lett. **69**, 1209 (1992).
- [14] Y. Kantor and D.R. Nelson, Phys. Rev. Lett. **58**, 2774 (1987); Phys. Rev. A **36**, 4020 (1987).
- [15] M. Baig, D. Espriu, and J. Wheeler, Nucl. Phys. B **314**, 587 (1989); J. Ambjørn, B. Durhuus, and T. Jonsson, Nucl. Phys. B **316**, 526 (1989); R. Renken and J. Kogut, Nucl. Phys. B **342**, 753 (1990); R. Harnish and J. Wheeler, Nucl. Phys. B **350**, 861 (1991); J. Wheeler and P. Stephenson, Phys. Lett. B **302**, 447 (1993); D. Espriu and A. Travesset, Nucl. Phys. B **468**, 514 (1996).
- [16] J.-P. Kownacki and H.T. Diep, Phys. Rev E **66**, 066105 (2002); H. Koibuchi, N. Kusano, A. Nidaira, K. Suzuki, and M. Yamada, Phys. Rev. E **69**, 066139 (2004); H. Koibuchi and T. Kuwahata, Phys. Rev. E **72**, 026124 (2005).
- [17] J.-P. Kownacki and D. Mouhanna, Phys. Rev E **79**, 040101R (2009).
- [18] A. Cappi, P. Colangelo, G. Gonnella and A. Maritan, Nucl. Phys. B **370**, 659 (1992).
- [19] E.N.M. Cirillo, G. Gonnella, D.A. Johnston, and A. Pelizzola, Phys. Lett. A **226**, 59 (1997).
- [20] M. Bowick, P. Di Francesco, O. Golinelli and E. Guitter, Nucl. Phys. B **450**, 463 (1995).
- [21] Y. Kantor and M.V. Jarić, Europhys. Lett. **11**, 157 (1990).
- [22] P. Di Francesco and E. Guitter, Europhys. Lett. **26**, 455 (1994).
- [23] P. Di Francesco and E. Guitter, Phys. Rev. E **50**, 4418 (1994).
- [24] E.N.M. Cirillo, G. Gonnella, and A. Pelizzola, Phys. Rev. E **52**, 1479–1484 (1996).
- [25] Y. Nishiyama, Phys. Rev. E **82**, 012102 (2010).
- [26] P. Di Francesco, Nucl. Phys. B **525**, 507 (1998); *ibid.* **528**, 453 (1998).
- [27] E.N.M. Cirillo, G. Gonnella, and A. Pelizzola, Nucl. Phys. B **583**, 584 (2000).
- [28] P. Di Francesco, E. Guitter and S. Mori, Phys. Rev. E **55**, 237 (1997).
- [29] S. Mori and E. Guitter, J. Phys. A: Math. Gen. **30**, L829 (1997).
- [30] E.N.M. Cirillo, G. Gonnella, and A. Pelizzola, Phys. Rev. E **53**, 3253–3256 (1996).
- [31] M. Bowick, O. Golinelli, E. Guitter, S. Mori, Nuclear Physics B **495**, 583–607 (1997).
- [32] A. Pelizzola, J. Phys. A: Math. Gen. **38** R309 (2005).



- [33] Y. Nishiyama, Phys. Rev. E **70**, 016101 (2004).
- [34] Y. Nishiyama, Phys. Rev. E **72**, 036104 (2005).
- [35] Y. Nishiyama, Phys. Rev. E **81**, 041116 (2010).
- [36] We also studied a different model where the defects corresponding to separate violations of the folding rules (2.5) and (2.6) ( $c=1,2$ ) are weighted by distinct energy costs. The resulting phase diagram is qualitatively very similar to that shown in Fig. 3, the only qualitative change being the disappearance of a tricritical point on the flat–octahedral transition line.
- [37] See, e.g., R.J. Baxter, *Exactly Solved Models in Statistical Mechanics* (Academic, London 1982).

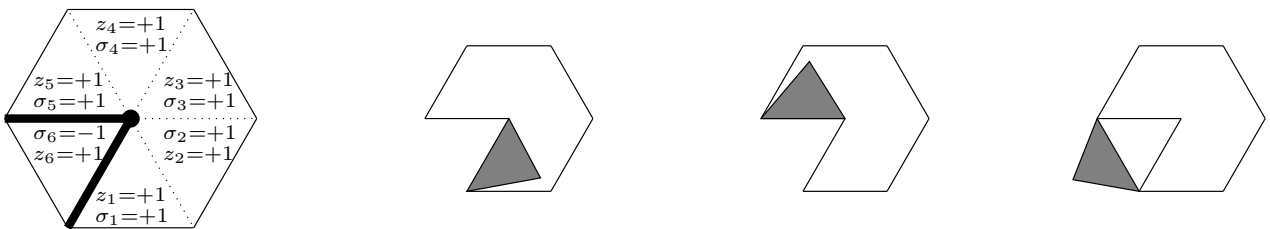


FIG. 1. On the left: a hexagon configuration with a complete fold domain wall represented by the thick line between  $(\sigma, z) = (+1, +1)$  and  $(-1, +1)$ . On the right: the three possible surface folded configurations corresponding to the hexagon spin configuration on the left, obtainable by cuts in the original triangular network as described in the main text.



FIG. 2. Two different hexagon configurations where a complete fold, a tetrahedral and an octahedral domain wall (respectively represented by lines of decreasing thickness) meet at the center of the hexagon. The octahedral and the complete fold domain walls are swapped in the two configurations.

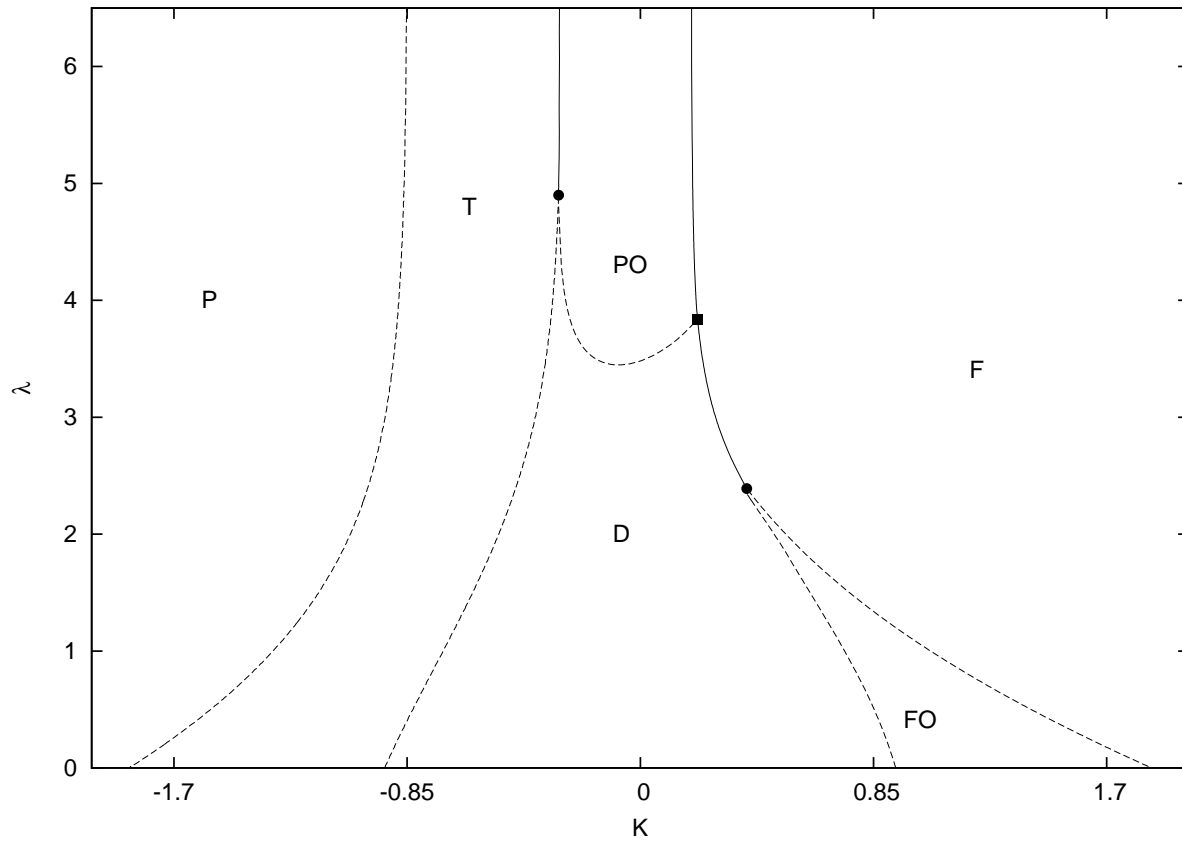


FIG. 3. Phase diagram of the model Eq. (2.7), where P, T, PO, D, FO, and F stand respectively for piled-up, tetrahedral, piled-octahedral, disordered, flat-octahedral, and flat. The solid circles and the solid box denote, respectively, the bicritical points and the critical end-point. Solid and dashed lines denote, respectively, first-order and continuous transitions.

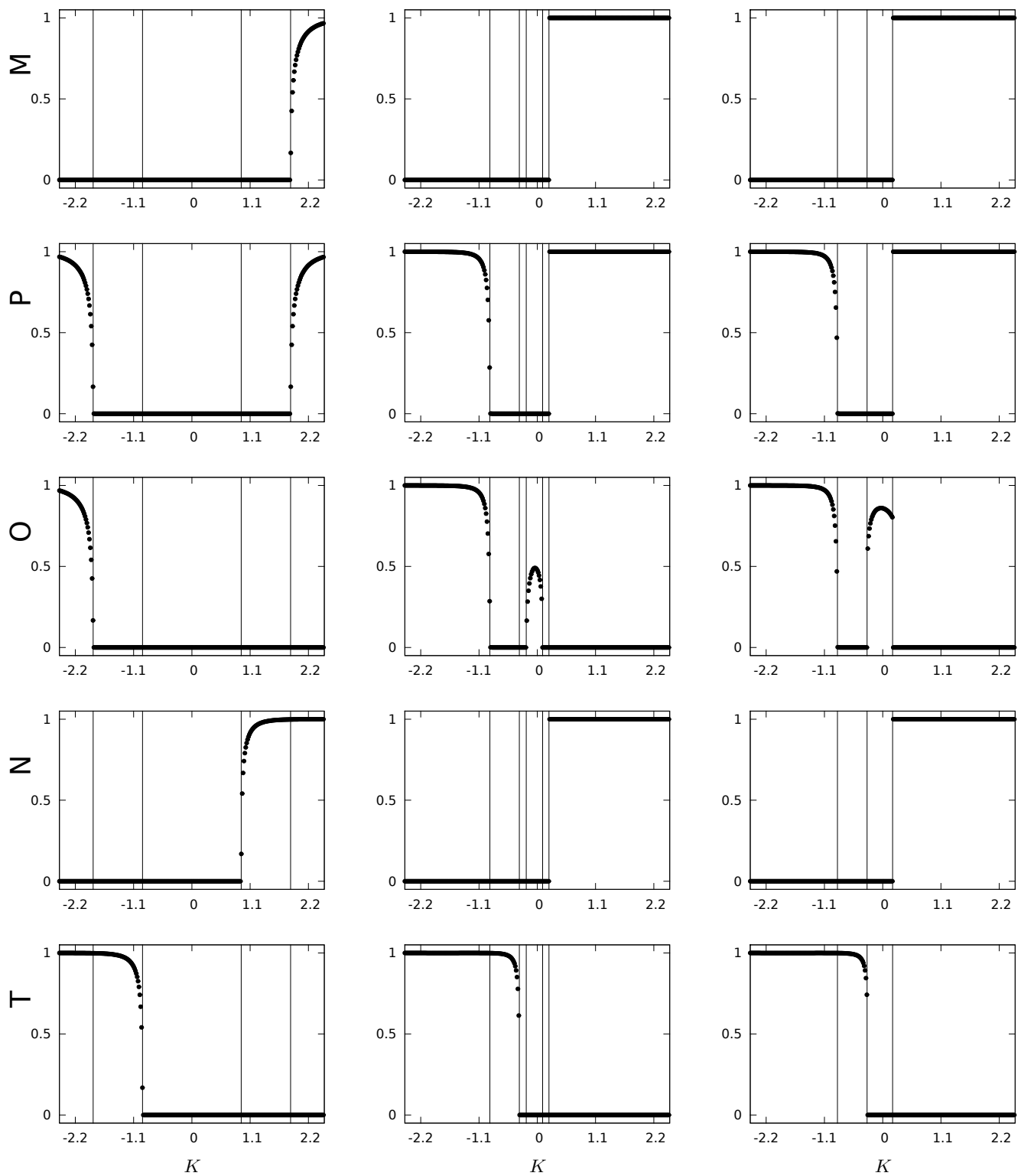


FIG. 4. Order parameters vs.  $K$  for different values of the constraint parameter  $\lambda$ . From the left to the right  $\lambda$  takes the values 0, 3.6, and 6. The thin vertical lines indicate points where a phase transition occurs. From the left to the right the phases are piled-up, tetrahedral, disordered, flat-octahedral, and flat at  $\lambda = 0$ , piled-up, tetrahedral, disordered, piled-octahedral, disordered, and flat at  $\lambda = 3.6$ , piled-up, tetrahedral, piled-octahedral, and flat at  $\lambda = 6$ .

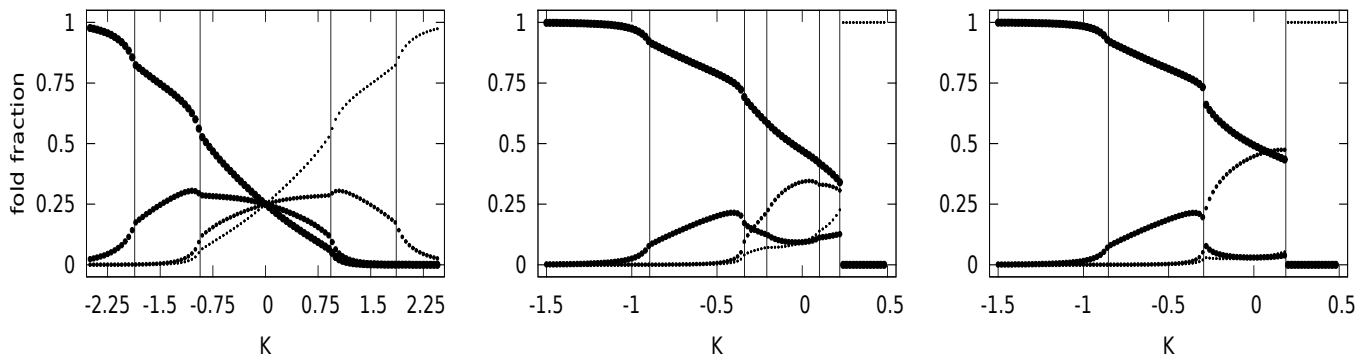


FIG. 5. Different fold fractions. From the left to the right  $\lambda$  takes the values 0, 3.6, and 6. The thin vertical lines indicate points where a phase transition occurs. From the left to the right the phases are piled-up, tetrahedral, disordered, flat-octahedral, and flat at  $\lambda = 0$ ; piled-up, tetrahedral, disordered, piled-octahedral, disordered, and flat at  $\lambda = 3.6$ ; piled-up, tetrahedral, piled-octahedral, and flat at  $\lambda = 6$ . The dotted lines, in increasing thickness order, denote respectively no fold, octahedral fold, tetrahedral fold, and complete fold.

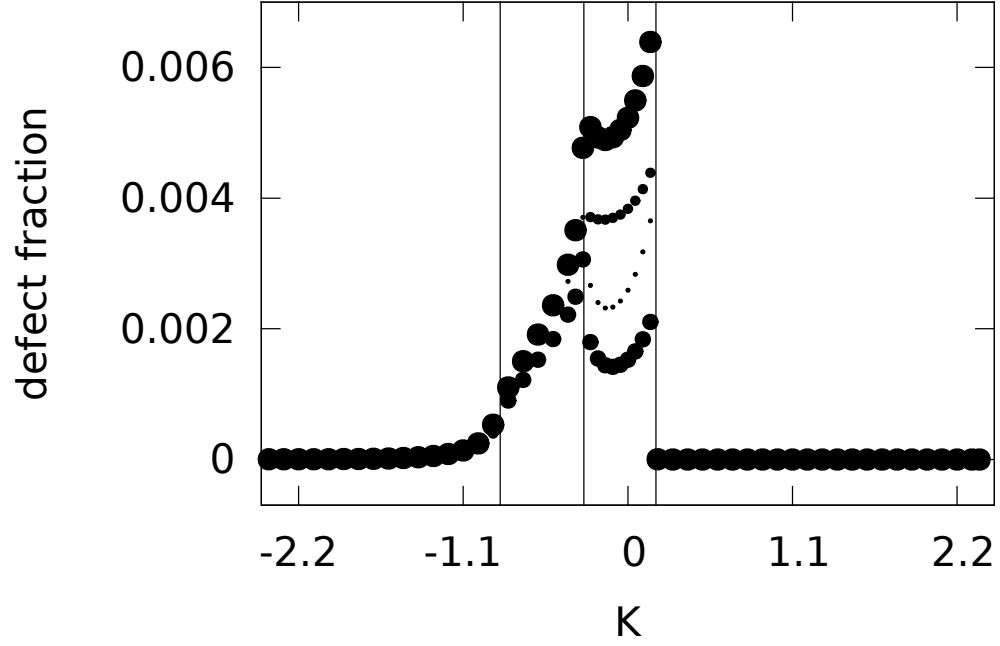


FIG. 6. Fraction of defects as a function of  $K$  for  $\lambda = 6$ . The dotted lines, in increasing thickness order, denote respectively  $p_L$ ,  $p_{M_1}$ ,  $p_{M_2}$ , and  $p$ . The thin vertical lines indicate points where a phase transition occurs. From the left to the right the phases are piled-up, tetrahedral, piled-octahedral, and flat.

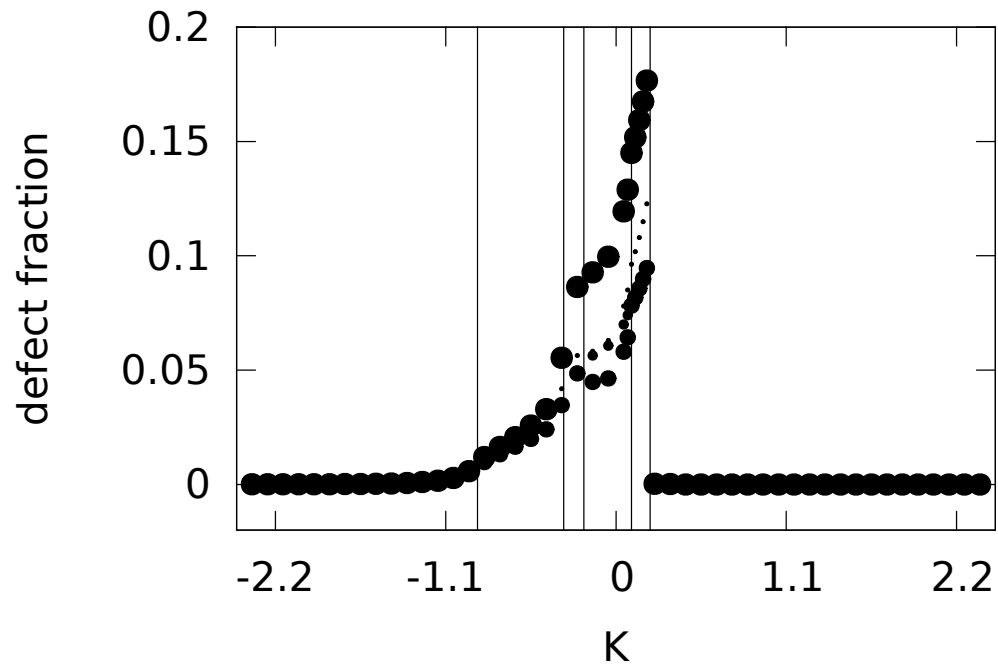


FIG. 7. Same as Fig. 6 for  $\lambda = 3.6$ . From the left to the right the phases are piled-up, tetrahedral, disordered, piled-octahedral, disordered, and flat.



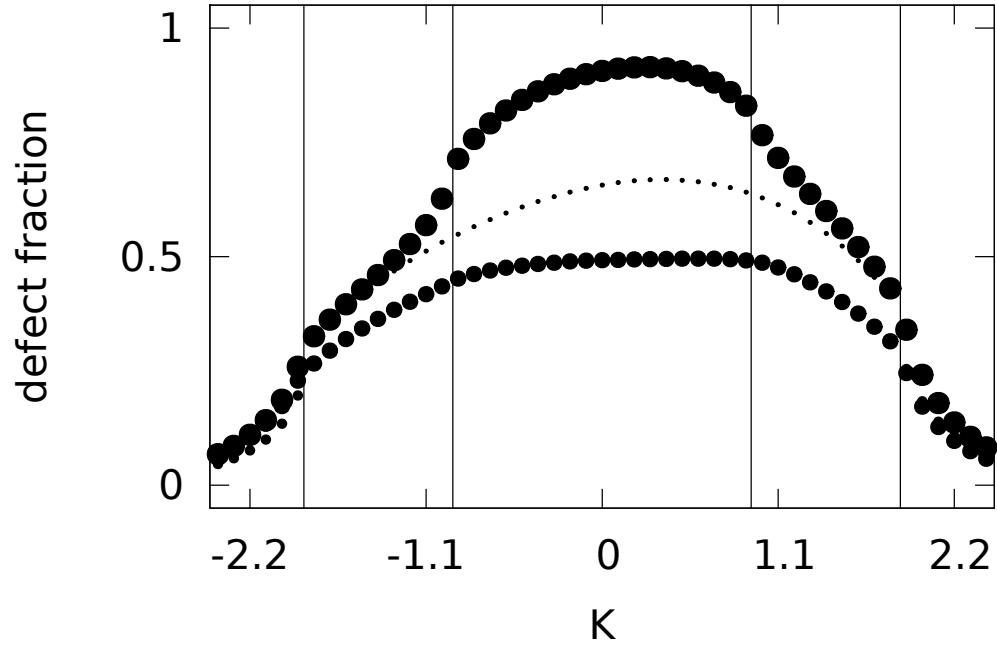


FIG. 8. Same as Fig. 6 for  $\lambda = 0$ . From the left to the right the phases are piled-up, tetrahedral, disordered, flat-octahedral, and flat.